Modelling building airtightness pressurisation tests with periodic wind and sharp-edged openings

François Rémi Carrié, Adeline Mélois

▶ **To cite this version:**

François Rémi Carrié, Adeline Mélois. Modelling building airtightness pressurisation tests with periodic wind and sharp-edged openings. Energy and Buildings, 2020, 208, pp.109642 -. 10.1016/j.enbuild.2019.109642 . hal-03488772

HAL Id: hal-03488772
https://hal.science/hal-03488772

Submitted on 21 Jul 2022

HAL is a multi-disciplinary open access archive for the deposit and dissemination of scientific research documents, whether they are published or not. The documents may come from teaching and research institutions in France or abroad, or from public or private research centers.

L'archive ouverte pluridisciplinaire **HAL**, est destinée au dépôt et à la diffusion de documents scientifiques de niveau recherche, publiés ou non, émanant des établissements d'enseignement et de recherche français ou étrangers, des laboratoires publics ou privés.

Distributed under a Creative Commons Attribution - NonCommercial 4.0 International License

Version of Record: https://www.sciencedirect.com/science/article/pii/S0378778819323709
Manuscript_7fadf5f00c6f2164785e407411ff70aa

Modelling building airtightness pressurisation tests with periodic wind and sharp-edged openings

François Rémi Carrié[1], Adeline Mélois[2,3]

1 ICEE
93 rue Molière
69003 Lyon, France
e-mail: remi.carrie@icee-energy.eu
Tel: +33 9 70 40 64 22
Fax: +33 9 57 38 91 31

2 Cerema BPE Project team
46 rue Saint Théobald
38081, L'Isle d'Abeau, France
e-mail: adeline.melois@cerema.fr
Tel: +33 4 74 27 53 08

3 ENTPE – University of Lyon, LTDS,
3 rue Maurice Audin, ,
69120 Vaulx-en-Velin, France

© 2019 published by Elsevier. This manuscript is made available under the CC BY NC user license
https://creativecommons.org/licenses/by-nc/4.0/

ABSTRACT

This paper presents an approach to model building airtightness pressurisation tests and to quantify uncertainties due to a periodic wind. Our approach assumes the building under test can be represented as a single zone with two sharp-edged openings, one on the windward side and one on the leeward side of the building. We detail the system of equations obtained which deals with stack effect, air compressibility, and inertia of the air subjected to unsteady pressure conditions at the boundaries of the openings. Solving the system of equations gives the dynamic behaviour of the airflow rates and state variables in the enclosure and in the leaks, making it possible to estimate the uncertainty of the air leakage coefficient in one-point pressurisation tests. Our analyses show that: a) the wind fluctuations can yield much larger uncertainties on the air leakage coefficient than the average wind alone; b) the wind frequency influences significantly the uncertainty when it is smaller than the sampling frequency; and c) the contribution of the zero-flow pressure uncertainty to the uncertainty of leakage airflow rate error is of about the same size as that of the flow and pressure uncertainties at the pressure measurement station.

KEYWORDS

Airtightness; air leakage; building; pressurisation test; infiltration; periodic wind

HIGHLIGHTS

- We present an approach to model building airtightness pressurisation tests and to quantify uncertainties due to a periodic wind.
- The approach, based on an idealised building and physical models of the airflow rate through the leaks, gives the airflow rates and state variables as a function of time.
- Our analyses show the limitations of steady-wind approaches.

NOMENCLATURE

A	Area of opening (m^2)

Subscripts and superscripts

1,2	Pertaining to opening number 1 or 2

c	Speed of sound $\left(=\sqrt{\gamma\, R\, T_e}\right)$ (m s^{-1})
c_p	Specific heat capacity at constant pressure (= 1 004 J kg^{-1} K^{-1})
c_v	Specific heat capacity at constant volume $\left(=1.4\, c_p\right)$ (J kg^{-1} K^{-1})
C_l	Air leakage coefficient at standard conditions (m^3 s^{-1} Pa^{-n})
C_p	Wind pressure coefficients defined in Table 2 (-)
C_{pw}	Wind pressure coefficients (-)
C_z	Discharge coefficients (-)
f_w	Wind frequency (s^{-1})
F	Coefficient defined in Table 2 (-)
Fr	Froude number (-)
g	Acceleration of gravity (= 9.81 m s^{-1})
G	Coefficient defined in Table 2 (-)
L	Length (m)
L_{build}	Reference building length (m)
Ld	Leakage distribution ratio (-)
l_e	Effective length of opening (m)
n	Flow exponent (-)
n_p	Polytropic exponent (-)
p_{abs}	Absolute pressure (Pa)
p	Pressure relative to external atmospheric pressure (Pa)
q	Volumetric airflow rate (m^3 s^{-1})
q_l	Volumetric airflow rate at standard conditions (m^3 s^{-1})
R	Specific gas constant (= 287.058 J kg^{-1} K^{-1})
t	Time (s)
T	Temperature (K)
U	Wind speed at the building level (m s^{-1})
$u(x)$	Uncertainty of a quantity x (units of x)
V_i	Internal building volume (m^3)
z	Altitude above ground level (m)

pd	Pertaining to pressurisation measurement device
down	Pertaining to leeward façades
e	Pertaining to outside the building
est	Estimated value
f	Pertaining to wind fluctuations
i	Pertaining to inside the building
l	Pertaining to leakage path
l	Pertaining to leakage path
mean	Mean value
nowindstack	No wind or stack effect
ref	Referring to reference
s	Referring to target pressure station
spl	Referring to values averaged over sampling interval
up	Pertaining to windward façades
w	Pertaining to wind
zf	Zero-flow pressure measurement
*	Non-dimensional quantity
0	Referring to standard conditions (293.15 K, 101325 10^5 Pa)

Greek symbols

$\delta(x)$	Error of x (units of x)
$\Delta(x)$	Difference in the value of x between the outside and the inside of the building (Pa)
Φ	Heat flux (W)
γ	Ratio of specific heats ($\gamma = \frac{c_p}{c_v} = 1.4$)
ρ	Air density (kg m^{-3})
φ	Phase lag (s)

Terms

Error (of a quantity)	Measured quantity value minus a reference quantity value
Uncertainty (of a quantity)	Dispersion of values that could be reasonably attributed to the quantity of interest

Sign convention

The air flow rates are counted positive when air travels from outside to inside

1 INTRODUCTION

Airtightness is an important building characteristic that influences the amount of air passing through building zones and walls. This is why there exists a significant body of literature dealing with building airtightness impacts on energy use [1–6] and indoor air quality [5,7]. The general consensus that can be drawn is that, except maybe in mild climates without cooling needs or moisture issues, building airtightness can greatly affect energy performance and indoor air quality. Because the energy use impact is proportionally more significant in low energy buildings which many policies aim to generalise to answer energy conservation and climate change issues, an increasing number of regulations and programmes have recently included requirements on building airtightness [8,9]. These regulations can include requirements for minimum airtightness or default values that strongly penalise poor airtightness; they can also include quality management requirements aiming at securing good airtightness [10].

In this context, quantifying airtightness has become a key issue for building professionals because failure to reach minimum targets can have significant legal and financial consequences. Subsequently, there has been over the past 10 years a revived interest among researchers and professionals concerning the reliability of pressurisation tests performed to quantify building airtightness. On the practical side, this has led to revise the international standard to perform building pressurisation tests (ISO 9972) [11] as well as a range of additional details spelled out at national or local levels to specify conditions to perform such a test, including certification programmes for testers [12]. As for the ASTM E779 standard commonly used in North America, it has been revised in 2019 [13]. On the research side, several authors have recently investigated uncertainties in building pressurisation tests [14–18], building on previous work performed in the 1980s and 1990s including evaluations of the impact of climatic conditions, calibration and variation on the value of the flow exponent [19–29]. Note that pressurisation tests are commonly performed at a single or a series of pressure

62 stations. These are also called DC pressurisation tests. However, considerable research and
63 development are ongoing on pulse pressurisation [30], an alternative method consisting in
64 analysing the pressure decay of a pulse released in an enclosure to derive its airtightness
65 characteristics at low pressure.
66
67 More specifically on wind induced uncertainties in DC pressurisation tests , Modera and
68 Wilson (1990) [25] recommend four-surface pressure averaging and time-averaging of
69 pressure and airflow data to reduce scatter in windy conditions. Later, Walker et al. (2013)
70 [14] and Carrié and Leprince (2014; 2016) [15,31] have analysed the impact of wind on
71 uncertainties based on large experimental datasets for the former and an analytical model for
72 the latter. Walker et al. (2013) recommend multipoint testing at low wind speeds (< 3 m s^{-1})
73 when the reference pressure is 4 Pa to avoid extrapolation errors due a fixed flow exponent;
74 however, for the same reference pressure (4 Pa), both Walker et al. (2013) and Carrié and
75 Leprince (2016) recommend single point-testing at high wind speeds (above 5-6 m s^{-1})
76 because using a default value of the flow exponent is better than trying to estimate it with low
77 pressure points. Prignon *et al.* (2019) [32] have investigated uncertainties in zero-flow
78 pressure measurements and have concluded that, because these could seriously impact
79 pressurisation test results, these should be accounted for in test standard ISO 9972. However,
80 to our knowledge, understanding the physics involved in the influence of wind on building
81 pressurisation tests remains unclear. There exists a threshold for the zero-flow pressure in ISO
82 9972 (5 Pa) beyond which the test is not valid. A wind speed of 6 m s^{-1} is mentioned in ISO
83 9972, but only to state that it is unlikely to have a zero-flow pressure of less than 5 Pa with
84 wind speed beyond that value. We are unaware of a thorough justification either for using the
85 zero-flow pressure criterion, or for linking a wind speed of 6 m s^{-1} to a zero-flow pressure of 5
86 Pa. Although the work of Carrié and Leprince (2014; 2016) gives a simple physical model

enabling the analysis of influencing parameters, one important limitation of their work lies in the hypothesis of a steady wind. In the field, it is well known that wind speed fluctuations influence pressure measurements used in the analysis of building pressurisation tests and therefore the resulting building airtightness results.

In two papers [33,34], Ethridge focusses on fluctuating wind pressures in a naturally ventilated enclosure with two openings. He lays down fundamental equations of four models to address his problem. The flow equations of the most rigorous model—the "Quasi-steady/Temporal inertia model"—are of interest to model other problems involving fluctuating wind pressures, including pressurisation tests with unsteady wind. Note also that in his book ([35], pp. 96-99), Ethridge explains how the quasi-steady assumption and time-averaging can influence the error in the airflow rate. He details the case of an orifice plate meter in a pipe and gives the error in the airflow rate as a function of the Strouhal number in that specific case. However, the natural ventilation and orifice plate meter problems tackled by Ethridge [33,34] are clearly different from that of a pressurisation test involving air forced into or out of an enclosure by a pressurisation device and multiple openings subjected to different pressures because of wind and stack effects.

In summary, we are unaware of previous work to model pressurisation tests with unsteady winds or to analyse the uncertainty due to wind in such tests. The present paper extends Carrié and Leprince's model in order to characterise the influence of periodic wind on building one-point pressurisation tests with leaks acting as perfect orifices. We start with physical equations that give the airflow rates in cracks with unsteady pressure boundary conditions in an idealised building and analyse the results of our physical model for several cases.

2 QUASI-STEADY TEMPORAL INERTIA MODEL EQUATIONS

2.1 Idealised building

In accordance with Carrié and Leprince (2016), we assume that the building can be represented by a single zone separated from the outside by two types of walls: walls on the windward side of the building which are subject to the same upwind pressure; and walls on the leeward side which are subject to the same downwind pressure (Figure 1). We further assume that all leaks on the windward (respectively, leeward) side can be represented as a single opening at a given height—e.g., z_1 if opening 1 is on the windward side (respectively, leeward) —subjected to the same pressure difference.

In the field, the roof, the sides (façades n°3 and n°4 in Figure 1) and the leeward façade (n° 2 in Figure 1) have negative pressure coefficients on average; the windward façade (n°1) has a positive pressure coefficient on average. In our idealised building, only one average pressure coefficient is considered for all leaks on the windward (resp. leeward) façades. Similarly, only one average height is considered for all leaks on the windward (resp. leeward) façades. This is of course a crude representation of the complexity of real airflow paths. Nevertheless, it has the advantage of remaining relatively simple while allowing us to calculate the airflow rates in leaks subjected to different pressures during a pressurisation test, which is the key problem in presence of wind. The system of interest can be represented as shown in Figure 1.

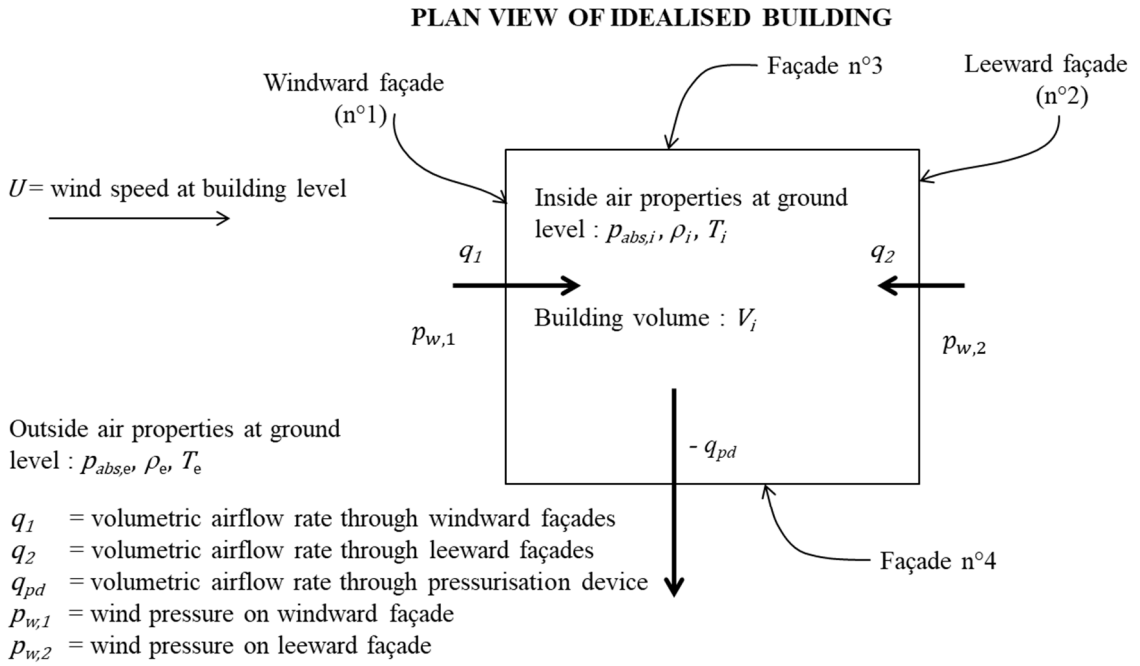

Figure 1: Plan view of idealised building with wind facing façade 1

2.2 Temperature and density of airflows entering and leaving the building

To remain consistent with the complexity level of our idealised building, we assign a density and temperature to the airflow paths entering or leaving the space as if air was directly transferred in or out of the enclosure, without interaction with the building fabric or pressurisation equipment. This leads to the equations detailed in Table 1.

Density	Eq. n°	Temperature	Eq. n°
$\rho_{pd} = \begin{cases} \rho_e & \text{if } sign(q_{pd}) \geq 0 \\ \rho_i & \text{if } sign(q_{pd}) < 0 \end{cases}$	(1)	$T_{pd} = \begin{cases} T_e & \text{if } sign(q_{pd}) \geq 0 \\ T_i & \text{if } sign(q_{pd}) < 0 \end{cases}$	(2)
$\rho_1 = \begin{cases} \rho_e & \text{if } sign(q_1) \geq 0 \\ \rho_i & \text{if } sign(q_1) < 0 \end{cases}$	(3)	$T_1 = \begin{cases} T_e & \text{if } sign(q_1) \geq 0 \\ T_i & \text{if } sign(q_1) < 0 \end{cases}$	(4)
$\rho_2 = \begin{cases} \rho_e & \text{if } sign(q_2) \geq 0 \\ \rho_i & \text{if } sign(q_2) < 0 \end{cases}$	(5)	$T_2 = \begin{cases} T_e & \text{if } sign(q_2) \geq 0 \\ T_i & \text{if } sign(q_2) < 0 \end{cases}$	(6)

Table 1: Density and temperature equations at airflow paths

2.3 Pressure difference at leakage sites

The pressure difference at the windward opening is:

$$\Delta p_1(t) = p_{w,1} - (\rho_e - \rho_i) g z_1 - p_i(t) \quad (7)$$

144

145 Similarly, at the leeward opening:

$$\Delta p_2(t) = p_{w,2} - (\rho_e - \rho_i) g z_2 - p_i(t) \quad (8)$$

146 **2.4 Flow through leakage sites**

147 In his analysis of unsteady flow effects due to fluctuating wind pressures, Ethridge (2000a,
148 2000b) [33,34] proposes to use a so-called "*Quasi-steady/Temporal inertia model*" (or *QT*
149 *model*) to describe the flow through the leaks. Applying the same approach in our case leads
150 to the following flow equations through the leaks:

$$2C_{z,1}A_1 l_{e,1} \frac{dq_1(t)}{dt} = -q_1^2(t)\, sign\left(q_1\ (t)\right) + 2C_{z,1}^2 A_1^2 \frac{\Delta p_1(t)}{\rho_1} \quad (9)$$

$$2C_{z,2}A_2 l_{e,2} \frac{dq_2(t)}{dt} = -q_2^2(t)\, sign\left(q_2\ (t)\right) + 2C_{z,2}^2 A_2^2 \frac{\Delta p_2(t)}{\rho_2} \quad (10)$$

151 We assume the cracks in the envelope behave like sharp-edged orifices the discharge
152 coefficient is commonly assumed to be 0.6:

$$C_{z,1} = C_{z,2} = 0.6 \quad (11)$$

Regarding the entry length, Ethridge (2000a) used Modera's experimental data (Modera, 1989) [36] to show that the opening diameter was a reasonable estimate of this parameter. Therefore, we write:

$$l_{e,1} = \sqrt{\frac{4\ A_1}{\pi}};\ l_{e,2} = \sqrt{\frac{4\ A_2}{\pi}} \quad (12)$$

2.5 Equation of state

We assume that the air behaves like a perfect gas, therefore:

$$p_{abs,0} = \rho_0 \, R \, T_0 \tag{13}$$

$$p_{abs,e} = \rho_e \, R \, T_e \tag{14}$$

$$p_{abs,i} = p_{abs,e} + p_i = \rho_i \, R \, T_i \tag{15}$$

2.6 Continuity equation

The mass air flow rates through the leakage sites and the pressurisation device are:

$$q_{m,pd} = \rho_{pd} \, q_{pd} \tag{16}$$

$$q_{m,1} = \rho_1 \, q_1 \tag{17}$$

$$q_{m,2} = \rho_2 \, q_2 \tag{18}$$

Writing the mass balance of the internal volume gives:

$$\frac{dm_i(t)}{dt} = V_i \frac{d\rho_i(t)}{dt} = q_{m,pd}(t) + q_{m,1}(t) + q_{m,2}(t) \tag{19}$$

2.7 Energy conservation equation

Ethridge (2000a; 2000b) assumes that the bulk behaviour of the internal volume follows a polytropic process, yielding:

$$\frac{P_i(t)}{\rho_i(t)^{n_p}} = K \tag{20}$$

where K is a constant. For a perfect gas, if the process is adiabatic, $n_p = \gamma$; whereas, if the process is isothermal, $n_p = 1$. In the adiabatic case, this relationship stems from applying the state equation and the first principle of thermodynamics to a closed system with homogeneous state variables. This assumption is convenient because it reduces the energy conservation equation to a simple mathematical form (equation (20)). Although the air pressure and temperature inside values differ from outside values, this assumption can be justified with the Boussinesq approximation—i.e., the density variations are considered only in the buoyancy terms, in other words, in the terms where gravity appears in equations (1) and (3)—and since the absolute pressure is nearly identical inside and outside the building (see Figure 2).

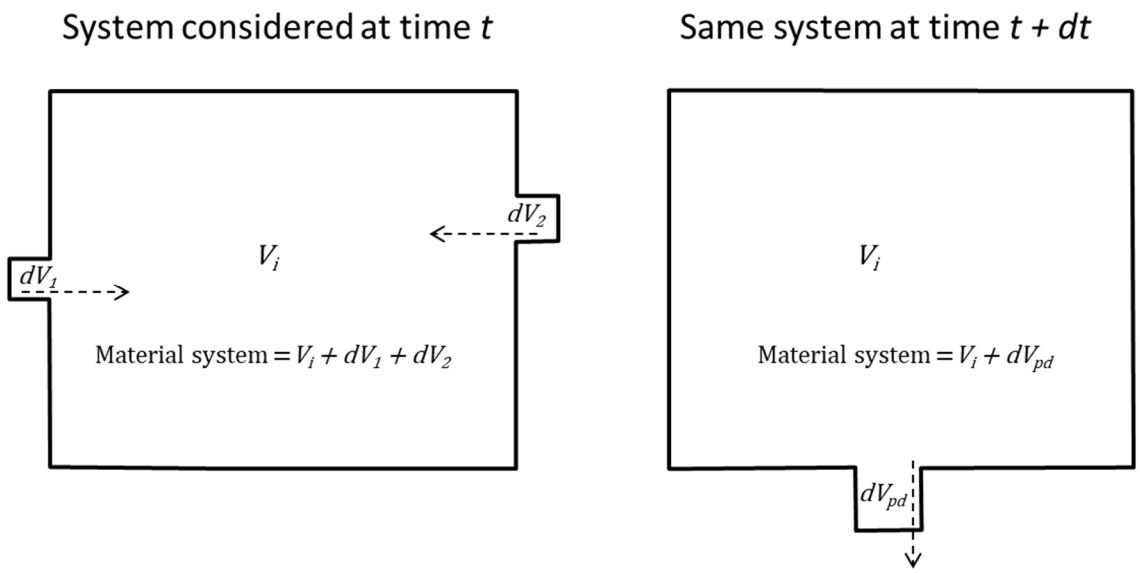

Figure 2: Closed system considered with the Boussinesq approximation and with $P_i \approx P_e$ (the air is assumed to enter the building through openings 1 and 2 and leave through the pressurisation device).

However, in the more general case, the internal volume is an open system and air at different temperatures flows in and out of this volume. When we apply the energy conservation principle to the internal volume, accounting for energy exchanges due to the air entering and leaving the building, but neglecting other energy transfer through the walls, mechanical stress or internal sources, we obtain:

$$V_i c_v \frac{d\left(\rho_i(t)\, T_i(t)\right)}{dt} = \Phi_{pd}(t) + \Phi_1(t) + \Phi_2(\mathrm{t}) \tag{21}$$

Where:

$$\Phi_{pd} = \rho_{pd}\, c_p\, q_{pd}\, T_{pd} \tag{22}$$

$$\Phi_1 = \rho_1\, c_p\, q_1\, T_1 \tag{23}$$

$$\Phi_2 = \rho_2\, c_p\, q_2\, T_2 \tag{24}$$

2.8 Zero-flow pressure

Depending on wind speed and temperature conditions, the pressure in the building when all intentional openings are closed is not null. This pressure is called the zero-flow pressure. It is subtracted from the measured pressures at the pressure stations to derive airtightness characteristics (see ISO 9972 [11] or ASTM E-779 [13]).

We obtain the zero-flow pressure with equations (1) through (19) and (21) through (24), where we set $q_{m,pd}$ to 0.

2.9 Leakage airflow rate error

Assuming a flow exponent of 0.5 (sharp-edged orifices), the estimated airflow rate through the leaks at the target pressure station is:

$$q_{l,est}(p_s) = C_{l,est}\sqrt{|p_s|}\ sign(p_s)\ , \tag{25}$$

where, accounting for temperature and pressure corrections as described by Carrié (2014) [37], the estimated leakage coefficient of the building for a one-point measurement test can be calculated as follows, in pressurisation mode:

$$C_{l,est} = -\sqrt{\frac{\rho_i}{\rho_0}} \frac{\frac{\rho_e}{\rho_i} q_{pd}}{\sqrt{|p_{zf}-p_i|}\ sign(p_{zf}-p_i)}, \quad (26)$$

200 and in depressurisation mode:

$$C_{l,est} = -\sqrt{\frac{\rho_e}{\rho_0}} \frac{\frac{\rho_i}{\rho_e} q_{pd}}{\sqrt{|p_{zf}-p_i|}\ sign(p_{zf}-p_i)} \quad (27)$$

201 The error in the estimated leakage airflow rate at the pressure station is:

$$\delta_r(q_l) = \frac{\delta q_l}{q_l} = \frac{q_{l,est} - q_{l,nowindstack}}{q_{l,nowindstack}} \quad (28)$$

202 where $q_{l,est}$ and $q_{l,nowindstack}$ are estimated at the same pressure. The leakage airflow rate in
203 no wind or stack effect condition $q_{l,nowindstack}$ is the leakage airflow rate that would be
204 observed in standard conditions applying a perfect orifice equation. It is obtained with
205 equation (25) by substituting $q_{l,est}$ and $C_{l,est}$ with $q_{l,nowindstack}$ and $C_{l,nowindstack}$ where:

$$C_{l,nowindstack} = \sqrt{\frac{2}{\rho_0}} \left(C_{z,1} A_1 + C_{z,2} A_2\right) \quad (29)$$

206

207 Note that, in the case of a pressurisation with a unique pressure station, we can infer the air
208 leakage coefficient error by calculating the error in the leakage airflow rate compared to no
209 wind or stack effect condition as follows:

$$\frac{\delta C_l}{C_l} = \frac{\delta q_l}{q_l} = \frac{C_{l,est} - C_{l,nowindstack}}{C_{l,nowindstack}} \quad (30)$$

210

211

212 **3 QUASI-STEADY COMPRESSIBLE AND ISOTHERMAL MODELS**

213 Based on the QT model equations detailed above, we have derived two other models with
214 additional assumptions. These additional models are simpler. They are meant to evaluate the

added-value of the complexity introduced with the inertia term in the flow equations, as well as with variable air density and temperature.

The “Quasi-steady Compressible” (QC) model neglects the inertia term in equations (9) and (10), i.e., the temporal derivative on the left-hand side of the equations. The temporal derivatives of the air density and pressure (equations (19)(21)) remain to be solved. Still, it reduces the dimension of system of ordinary differential equations from 4 in the QT model to 2.

Last, the “Quasi-Steady isothermal » (QS) model neglects the inertia term, the air compressibility, and temperature differences. By construction, this model violates the perfect gas law, therefore the equations listed in § 2.5 do not apply. Its key advantage is that its solution can be derived analytically, with an approach similar to that of Carrié and Leprince (2016).

Note that the QT and QC models defined in this paper are based on the same assumptions as those derived by Ethridge (2000a), except for the Boussinesq assumption and closed-system assumption implicit in the use of the polytropic law.

4 PRESSURISATION TEST CONDITIONS

4.1 Wind conditions

Users of the present model could use time series of upstream and downstream wind pressures measured simultaneously as model inputs. This could be interesting for comparing measured and model results for real test cases. However, to predict errors in the leakage airflow rates without wind pressure measurements on a specific test case, the users must assume a given

form for the wind pressure series. We are not aware of previous work giving simultaneous upstream and downstream wind pressures for given building characteristics, including the time lag, without wind measurements. To overcome this problem, we have assumed in such cases that the wind speed fluctuates around a mean value as follows:

$$U\ \ (t) = U_{mean}\left(1 + \frac{U_f}{U_{mean}} sin(2\pi\ f_w\ t)\right), \tag{31}$$

and that the wind pressures could be inferred from the wind speed with:

$$p_{w,1} = C_{pw,1}\frac{\rho_e\ U^2\ (t)}{2} \tag{32}$$

$$p_{w,2} = C_{pw,2}\frac{\rho_e\ U^2\ (t)}{2} \tag{33}$$

In other words, the wind speed fluctuation is reduced to a single mode of a Fourier transform and the wind pressures are derived from wind pressure coefficients available in the literature.

4.2 Sampling interval

ISO 9972 requires the zero-flow pressure to be measured over 30 seconds with at least 10 points but does not detail requirements for sampling intervals at pressure stations. In this paper, we chose to take the same sampling interval for the measurement at zero-flow and for the measurement at the pressure station.

4.3 Air temperature and pressure

The outside air temperature T_e and pressure $p_{abs,e}$ are constant during the pressurisation test. The difference between inside and outside air pressure is controlled by the pressurisation device (see § 4.4), whereas the inside air temperature is an output of the model.

4.4 Pressurisation device pressure control

We assume an ideal pressure control of the pressurisation device, i.e.:

$$\forall t, p_i(t) = p_s \tag{34}$$

In other words, at all times, the pressurisation device controller sets the building pressure to the target pressure station by ideally adjusting the pressurisation device airflow rate.

4.5 Initial conditions

In order to simulate pressurisation tests with the QT or QC models, one must specify initial conditions for the following internal air temperature and pressure, as well as for the leakage flows through the leaks and the pressurisation device.

Nevertheless, to avoid unrealistic behaviours of the internal air conditions and leakage airflows, we set the initial conditions to the values obtained after a time step short enough to have little variations of the state variables and a steady wind to avoid inertial effects in the leaks.

4.6 Range of input parameters

The sensitivity analysis performed further in this paper is restricted to the following ranges of the input parameters:

275 — The mean wind velocity U_{mean} varies between 0 and 10 m s^{-1};

276 — The wind fluctuation U_f is set to 20% of the mean value;

277 — The pressure measurement station is set to a target value of 10 or 50 Pa; or to the
278 maximum between those target pressures and a multiple of the zero-flow-pressure.
279 This latter option allows us to simulate the constraint $|p_s| \geq 5\,|p_{zf}|$ required in ISO
280 9972 for a test to be valid;

281 — The wind pressure coefficients are set to $C_{pw,1} = 0.25$ and $C_{pw,2} = -0.5$ inspired
282 from Liddament (1996) [38] (page 242, data for a low-rise building with a length-to-
283 width ratio of 2:1 and surrounded by obstructions equivalent to half of the building
284 height);

285 — The leakage distribution ratio $Ld = \frac{C_{z,2}\,A_2}{C_{z,1}\,A_1}$ is set to 4. Because we have one windward
286 façade and four leeward façades, this means that the leakage area is equally distributed
287 on all façades of the building;

288 — The initial air conditions are set to standard conditions;

289 — The outside air conditions are set either to standard conditions, or in anisothermal test
290 cases, with $T_e = 273.15\ K$.

291

292 We do not apply the zero-flow pressure constraint $|p_{zf}| \leq 5$ Pa set in ISO 9972 for the test to
293 be valid. This allows us to analyse the influence of the input parameters on the leakage
294 airflow rate error without discarding results *a priori*.

295

5 NON-DIMENSIONAL EQUATIONS

5.1 Dimensionless groups and reference values

The equations below are given in non-dimensional form, which reduces the number of inputs and unknowns and helps identify governing dimensionless variables. Let the non-dimensional numbers defined in the appendix. The reference values can be set arbitrarily, but it is convenient to define the reference wind pressure, $p_{w,ref}$, the reference wind speed, U_{ref}, and the reference length, L_{ref}, as follows:

$$p_{w,ref} = p_s \tag{35}$$

$$U_{ref} = \sqrt{\frac{2\,|p_{w,ref}|}{\rho_0}} = \frac{q_{pd,ref}}{\left(C_{z,1}\,A_1 + C_{z,2}\,A_2\right)} \tag{36}$$

$$L_{ref} = \frac{V_i}{\left(C_{z,1}\,A_1 + C_{z,2}\,A_2\right)} \tag{37}$$

This choice of reference values implies that:

— the relative pressures, including the pressure exerted by the wind on the façades, are compared to the pressure set by the pressurisation device;

— the wind velocity is compared to the velocity of the air passing through the leaks;

— the time is compared to the characteristic time of air renewal of the enclosure during the pressurisation test, $\frac{V_i}{q_{pd,ref}}$.

5.2 Key QT-model equations

With the non-dimensional groups defined in the appendix and reference values defined in § 5.1, the non-dimensional pressure differences and airflow rates at the leakage sites are:

$$\Delta p_1^* = C_{p,1} - \frac{2}{Fr_1^2}\,(\rho_e^* - \rho_i^*) - C_{p,i} \tag{38}$$

$$\Delta p_2^* = C_{p,2} - \frac{2}{Fr_2^2}\,(\rho_e^* - \rho_i^*) - C_{p,i} \tag{39}$$

$$\frac{dq_1^*}{dt^*} = \frac{F_1}{2}\left(-q_1^{*2}\,sign(q_1^*) + \frac{\Delta p_1^*}{\rho_1^*}\right) \tag{40}$$

$$\frac{dq_2^*}{dt^*} = \frac{F_2}{2}\left(-q_2^{*2}\,sign(q_2^*) + \frac{\Delta p_2^*}{\rho_2^*}\right) \tag{41}$$

314 The continuity and energy equations become:

$$\frac{d\rho_i^*}{dt^*} = \rho_{pd}^*\,q_{pd}^* + \frac{1}{1+Ld}\,\rho_1^*\,q_1^* + \frac{Ld}{1+Ld}\rho_2^*\,q_2^* \tag{42}$$

$$\frac{1}{2}\frac{1}{c^{*2}}\frac{d\left(C_{p,i}\right)}{dt^*} = \rho_{pd}^*\,T_{pd}^*\,q_{pd}^* + \frac{1}{1+Ld}\,\rho_1^*\,T_1^*\,q_1^* + \frac{Ld}{1+Ld}\,\rho_2^*\,T_2^*\,q_2^* \tag{43}$$

315 Assuming a closed system with homogenous state variables, which is implicit in the energy
316 equation (20) used by Ethridge (2000a), the dimensionless air densities and temperatures are
317 equal to unity. Logically, with this assumption and with only two openings (no pressurisation
318 device), the energy equation becomes strictly identical to the equation derived by Ethridge
319 (2000a) (QT model) (referenced (28) in his paper, with $L_{ref} = H$, see appendix).
320
321 When the pressure inside the building is perfectly controlled, the left hand-side of equation
322 (43) vanishes, yielding:

$$\rho_{pd}^{*}\, T_{pd}^{*}\, q_{pd}^{*} + \frac{1}{1+Ld}\, \rho_{1}^{*}\, T_{1}^{*}\, q_{1}^{*} + \frac{Ld}{1+Ld}\, \rho_{2}^{*}\, T_{2}^{*}\, q_{2}^{*} = 0 \tag{44}$$

323

324 Taking the resulting model as a whole, the dimensionless quantities during the measurement
325 (i.e., dimensionless airflow rate, pressure, temperature, and density) are function of 17
326 parameters:

$$\begin{aligned} &q_{pd}^{*}, T_{pd}^{*}, \rho_{pd}^{*}, q_{1}^{*}, T_{1}^{*}, \rho_{1}^{*}, q_{2}^{*}, T_{2}^{*}, \rho_{2}^{*}, p_{i}^{*}, T_{i}^{*}, \rho_{i}^{*} \\ &= f\left(t^{*}, U_{mean}^{*}, U_{f}^{*}, f_{w}{}^{*}, C_{pw,1}, C_{pw,2}, Fr_{1}, Fr_{2}, Ld, F_{1}, F_{2}, p_{s}^{*}, c^{*}, p_{abs,w}^{*}, p_{abs,e}^{*}, T_{e}^{*}, \rho_{e}^{*}\right) \end{aligned} \tag{45}$$

327 In addition, in equation (45), q_{pd}^{*} and p_{i}^{*} are linked by the pressurisation measurement
328 control. For the zero-flow pressure measurement, the device airflow rate is set to zero and the
329 output quantity of interest is the internal pressure, whereas for the measurement at the
330 pressure station, the internal pressure is controlled depending on the target pressure and the
331 output quantities of interest include in particular the airflow rate through the pressurisation
332 device.

333 **5.3 Uncertainty of zero-flow pressure and leakage airflow rate error**

334 Because in real conditions the zero-flow pressure is estimated with independent
335 measurements before and after the measurements at the pressure station, assuming the wind
336 probability distribution remains the same, the uncertainty of the zero-flow pressure is:

$$u\left(p_{zf}^{*}\right) = \frac{u\left(p_{zf,spl}^{*}\right)}{\sqrt{2}} \tag{46}$$

337 Equation (28) allows us to calculate the leakage airflow rate error for each measurement
338 point, which is identical to the leakage air coefficient error in a one-point measurement
339 pressurisation test. Using dimensionless variables, the relative error in the leakage airflow rate
340 for a given sampling interval and a given measured zero-flow pressure is, in pressurisation:

$$\delta_r(q_l) = -\sqrt{\rho^*_{i,spl}}\,\frac{\rho^*_e}{\rho^*_{i,spl}}\,q^*_{pd,spl}\sqrt{\frac{|p^*_s|}{|p^*_{zf}-p^*_{i,spl}|}}\,sign\left(p^*_{zf}-p^*_{i,spl}\right)-1 \qquad (47)$$

and, in depressurisation:

$$\delta_r(q_l) = -\sqrt{\rho^*_e}\,\frac{\rho^*_{i,spl}}{\rho^*_e}\,q^*_{pd,spl}\sqrt{\frac{|p^*_s|}{|p^*_{zf}-p^*_{i,spl}|}}\,sign\left(p^*_{zf}-p^*_{i,spl}\right)-1 \qquad (48)$$

where $\rho^*_{i,spl}$, $q^*_{bd,spl}$, and $p^*_{i,spl}$ are values averaged over the sampling interval. Note that there is an infinite number of possible values of the error $\delta_r(q_l)$ (and of p^*_{zf}) depending on when the sample starts relative to the wind fluctuations. In our case, the wind gives a leakage airflow rate error that has both: a random component that depends on when the zero-flow and pressure-station samples start relative to wind fluctuations; and, a systematic component due to the effect of wind which can be characterised with equations (47) and (48) for given sampling intervals. Here, the quantity of interest for our uncertainty analysis is the systematic component (the systematic error in the leakage airflow rate) and its associated uncertainty.

To find out a reasonable range of possible values of this leakage airflow rate error—that is, its uncertainty—with a perfect controller, we set $p^*_{i,spl} = p^*_s$ and we neglect air density variations which are expected to be small in the vast majority of test conditions. Therefore, in uncertainty analysis, $\delta_r(q_l)$ may be viewed as a function of $q^*_{pd,spl}$ and p^*_{zf}. Applying uncertainty analysis principles as described in "GUM - Guide to the expression of uncertainty in measurement"[39], assuming no correlation between the airflow rate and the zero-flow pressure, we obtain the uncertainty of $\delta_r(q_l)$ as follows:

$$u^2\left(\delta_r(q_l)\right) = \left|\frac{p^*_s}{p^*_{zf}-p^*_s}\right|u^2\left(q^*_{pd,spl}\right) + \frac{q^{*2}_{pd}}{4}\left|\frac{p^*_s}{\left(p^*_{zf}-p^*_s\right)^3}\right|u^2\left(p^*_{zf}\right) \qquad (49)$$

where p^*_{zf}, q^*_{pd} and their associated standard uncertainties represent the expected values of these quantities, i.e., their average value over possible sampling intervals.

5.4 Boundary conditions

The dimensionless wind velocity is:

$$U^*(t) = U^*_{mean} + U^*_f \sin(2\pi f^*_w t^*) \quad (50)$$

f^*_w is a dimensionless frequency also known as Strouhal number.

As for the pressure boundary conditions, the definitions of the reference wind speed and pressure yield:

$$C_{p,1} = C_{pw,1}\,\rho^*_e\,U^{*2} - p^*_s;\; C_{p,2} = C_{pw,2}\,\rho^*_e\,U^{*2} - p^*_s \quad (51)$$

The perfect pressurisation device controller gives:

$$p^*_i(t^*) = p^*_s \quad (52)$$

The boundary conditions for the outside air temperature and pressure, at any time, including t^*=0, are:

$$T^*_e = \frac{T_e}{T_0}, \quad (53)$$

$$p^*_{abs,e} = \frac{p_{abs,e}}{p_{abs,0}}, \quad (54)$$

whereas the inside air temperature and pressure boundary condition is only set for t^*=0:

$$T_i^*(t^* = 0) = \frac{T_i(t = 0)}{T_0} \tag{55}$$

$$p_{abs,i}^*(t^* = 0) = \frac{p_{abs,i}(t = 0)}{p_{abs,0}} \tag{56}$$

The model also requires initial conditions for the airflow rates through the pressurisation device and the leaks which are obtained as explained in § 4.5.

6 RESULTS ON TEST CASES

6.1 Code development and checking procedures

We have implemented the model equations detailed above in a numerical code in Python using the scipy package for the numerical integrator ("odeint" functions), with the range of input parameters given in § 4.6. While the kernel of the models implementation uses dimensionless variables, dimensional inputs/outputs can be specified/returned to compare our results with field experience.

It is good coding practice to cross-check the consistency of results obtained with various methods. In the following sub-sections, we have compared QT-model results obtained with the other models presented in § 3.

6.2 Anisothermal conditions

In our test cases, the external temperature remains constant over the measurement period. Therefore, as expected, the internal temperature converges towards the external temperature with our QT-model (Figure 3). In the test conditions of Figure 3, the temperature and the airflow rate through the pressurisation device take about two hours to converge. The resulting leakage airflow rate is over estimated by about 5% at the beginning of the simulation

compared to the true value, whereas it is underestimated by about 2% at the end of the simulation due to the wind effect alone (Figure 4). To obtain Figure 4, we had to assume a given zero-flow pressure. In our case, it was set to the mean zero-flow pressure in the test conditions of Figure 3 and on same simulation interval (7200 s). Note also, for code checking purposes, that the QT-, QC-and QS-model results shown in Figure 3 are consistent in isothermal conditions.

Anisothermal conditions influence pressurisation test results: depending on when the technician starts averaging results, the air temperature conditions change and thereby the measured zero-flow pressures or leakage airflow rates. Therefore, although there is no intrinsic limitation to our QT model for anisothermal conditions, such conditions considerably complicate the analysis of the results, including uncertainty estimates. For these reasons, the analyses of test cases in the following sub-sections focus on isothermal conditions.

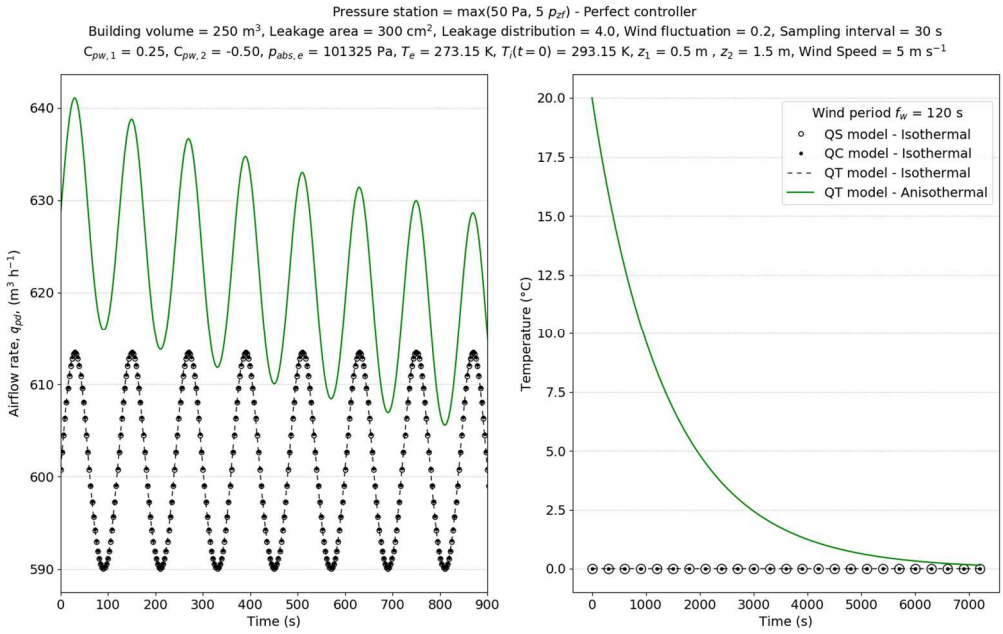

Figure 3: Leakage airflow rate and temperature time series in isothermal and anisothermal conditions (U_{mean} = 5 m s^{-1}, f_w = 120 s).

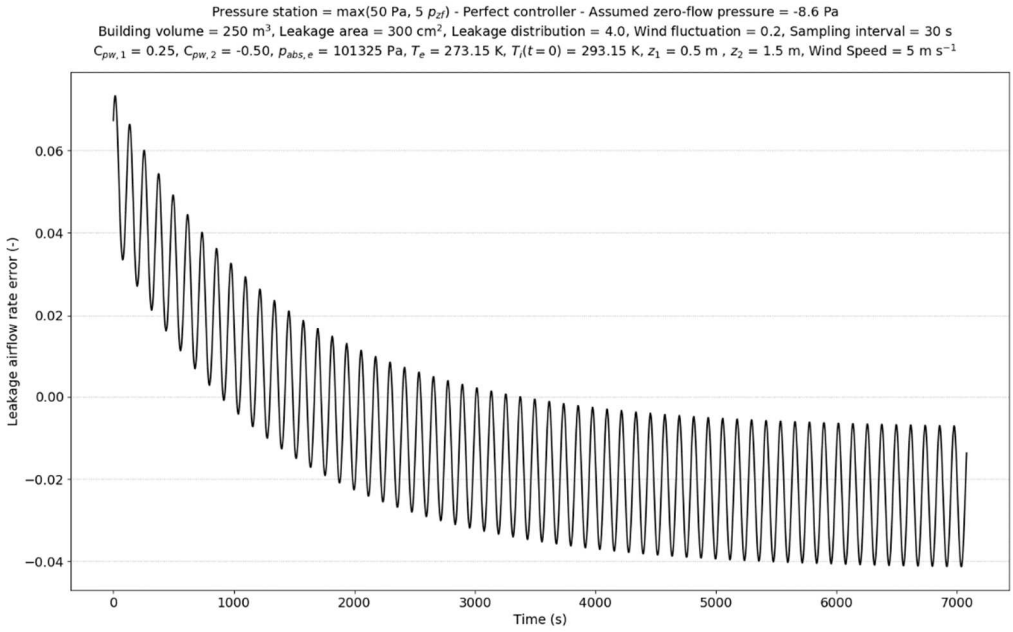

Figure 4: Leakage airflow rate error in anisothermal conditions (U_{mean} = 5 m s^{-1}, f_w = 120 s).

6.3 Inertia in the leaks

In the previous example, the QS, QC and the QT models give nearly identical results in isothermal conditions. However, for the zero-flow pressure time series, the inertial effects become visible at high frequencies as shown in Figure 5. We observe the same trend if we increase the building volume, which we expected from the dimensional analysis since the time derivatives of equations (40)(41) scale with F_1 and F_2 which increase with increasing volume. For the pressure station time series, we have to set the frequency or the building volume to higher values to observe similar trends as with the zero-flow pressure time series. This result is likely influenced by the pressure control strategy of the pressurisation device, i.e. the algorithm that controls the pressure during the test. Inertial effects could be more visible with more realistic control strategies because these yield an unsteady internal pressure. This would merit further research using realistic wind spectra to find out in which cases accounting for inertial effects is useful.

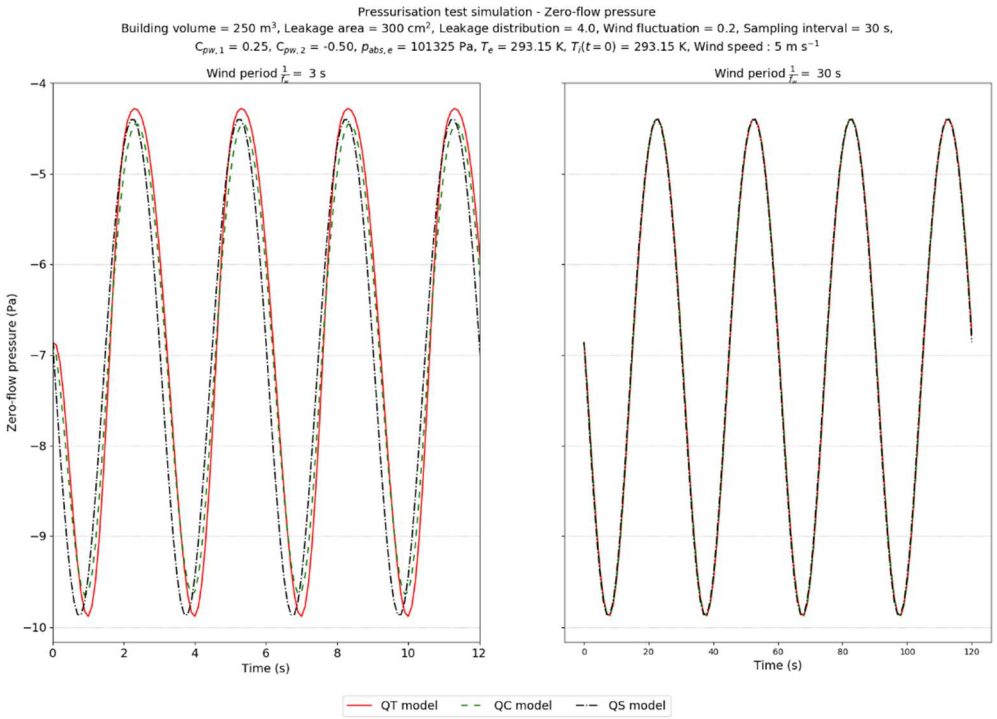

Figure 5: Zero-flow pressure time series (U_{mean} = 5 m s^{-1}, f_w = 3, 30 s).

6.4 Zero-flow pressure uncertainty

Figure 6 shows the standard uncertainty of the zero-flow pressures obtained from two sampling intervals. Logically, the uncertainty increases with decreasing wind frequencies: indeed, we expected the range to be small for wind periods smaller than the sampling time intervals because averages are biased when performed on sampling time intervals which are not multiples of the time period. This observation is consistent with the field results of Prignon et al. (2019) who concluded that longer sampling periods yielded lower uncertainties. Prignon's field measurements made under relatively low wind speeds (mean wind speed over 10 minutes lower than 3.8 m s^{-1}) showed estimates on the order of 0.4-1.5 Pa of the zero-flow pressure standard uncertainty. However, we must exercise caution comparing these field results with our numerical results because of model limitations (e.g., wind modelling with a sinusoidal signal versus real wind with many modes and changes in direction) and several inputs not assessed in the field, including: wind fluctuation amplitude, pressure coefficients, or leakage distribution. For these reasons, we have not tried to match our test cases with the inputs available from Prignon's study.

For our test conditions, our QT model gives zero-flow pressure standard uncertainties in the range of 0.3-2 Pa for wind speeds in the range 3-6 m s^{-1} and wind periods larger than the sampling time intervals, as shown in Figure 6. This figure also shows that the standard uncertainty can be much greater, for instance, greater than 5 Pa for low-frequency winds (or high wind periods) at 10 m s^{-1}.

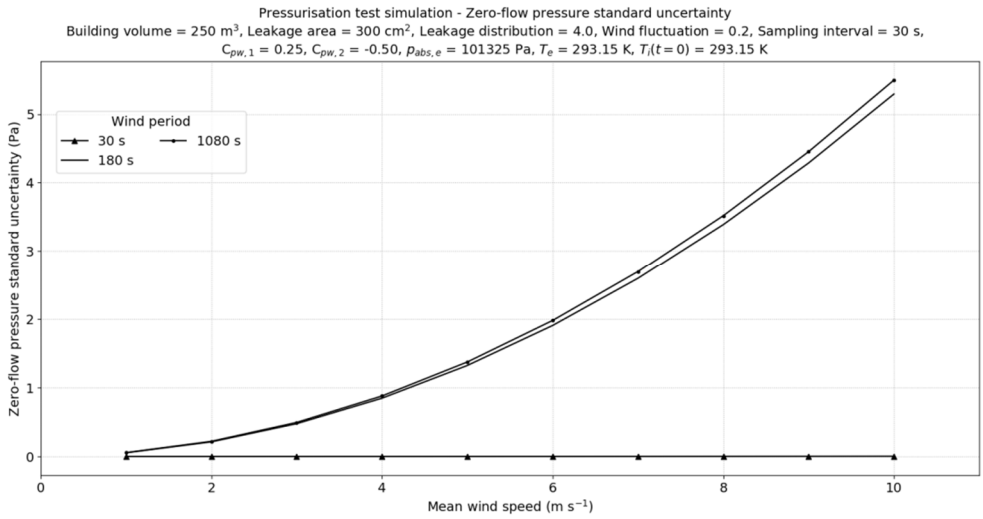

Figure 6: Zero-flow pressure standard uncertainty (averaged over 2 sampling intervals) as a function of wind speed for various wind periods.

6.5 Leakage airflow rate error

Figure 7 shows the leakage airflow rate times series for various wind frequencies as well as the uncertainty estimated with equation (49). The smaller bars represent the uncertainty in the error due to the zero-flow contribution, while the triangles represent that of the leakage airflow rate at the pressure station. In these specific cases, the contributions of the zero-flow pressure measurement (third term of equation (49)) and the leakage airflow measurement (second term of equation (49)) at the pressure station to the combined uncertainty of the leakage airflow rate error are comparable (Figure 7). In Figure 7, as logically as for the zero-flow pressure uncertainty, the uncertainty of the leakage airflow rate error increases with increasing wind periods (or decreasing wind frequencies).

Note also that, for code checking purposes, our QT-model results with $U_f = 0$ and those obtained with the steady model developed by Carrié and Leprince (2016) are identical.

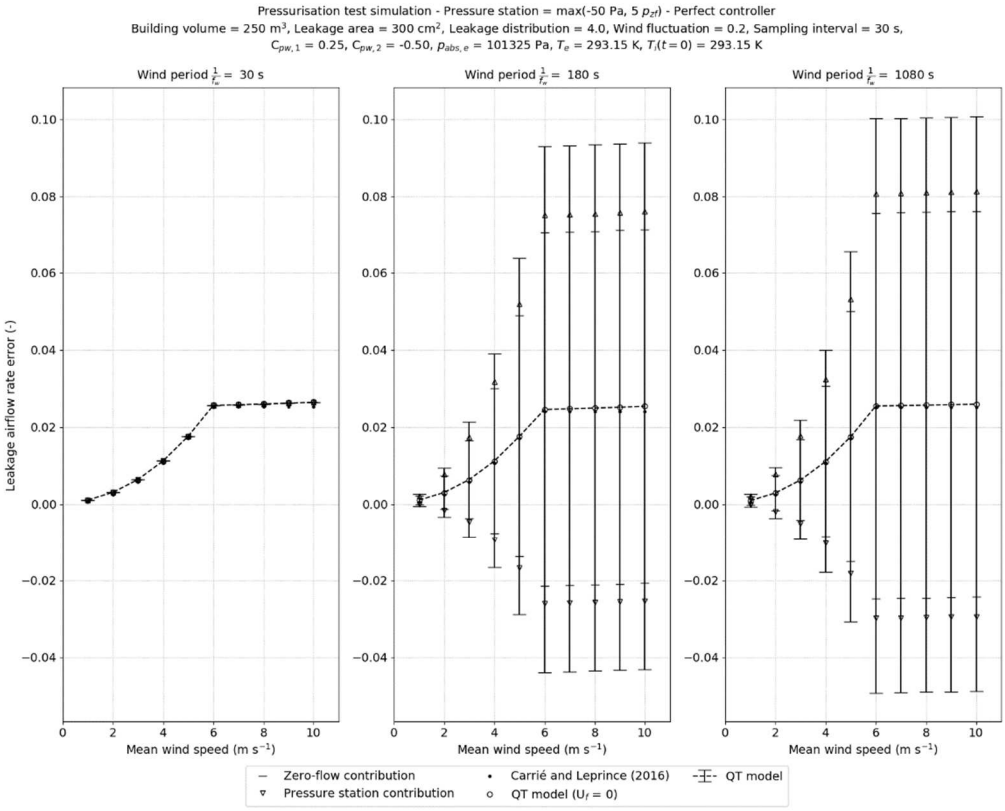

Figure 7: Leakage airflow rate error for various wind speeds and wind periods. The larger bars represent the uncertainty (coverage factor = 2) in the error due to wind fluctuations.

7 DISCUSSION

Experienced technicians are aware of specific difficulties to obtain repeatable results when performing pressurisation tests in windy conditions, including stable zero-pressure, pressure station and flow readings. This was reported by several authors, sometimes with diverging conclusions regarding the influence of wind. For instance, Persily (1982) [19] reports errors of 15% for an average wind speed of 4.9 m s^{-1} measured 6 m above the roof of a 2-storey building, whereas Brennan et al. (2013) [40] did not find a clear bias due to wind for wind

481 speeds up to about 10 m s^{-1}. Although surprising, these diverging results could be due to the
482 specificities of the test cases, i.e., diverging parameters that strongly influence the leakage
483 airflow rate error including wind fluctuation amplitude, pressure coefficients, leakage
484 distribution, or leakage area as shown in our analyses.
485
486 Although we observe some deviation between the QT and QC models at high wind
487 frequencies and low building airtightness, the added-value of the QT model is not obvious in
488 our test cases. Note however that these conclusions should not be extended beyond our test
489 cases. In particular, more realistic control strategies yielding short term variations of the
490 leakage airflow rate could show more clearly inertia flow effects in the leaks. This applies to
491 pressurisation at a given pressure station (also called DC pressurisation), but implementing
492 appropriate control strategies would also allow one to simulate AC or Pulse pressurisation
493 [30,41–43]using the key model equations detailed in this paper.
494
495 The models detailed in this paper assume perfect sharp-edged orifices and a rough estimate of
496 the entry length which is a key parameter influencing inertial effects. In addition, the simple
497 representation of parallel orifices with one single orifice questions the validity of Equation
498 (12) to give a proper estimate of the entry length. Because we have a non-linear system of
499 differential equations, it is not possible to extrapolate our results based on two sharp-edged
500 orifices to alternate flow models. Modified flow equations based on power law or a quadratic
501 law could be useful to better represent the flow behaviour in an array of cracks. If work is
502 undertaken in this area, the results of Walker et al. (1998) [29] suggest that the priority should
503 be given to the power law approach.
504

One specific added-value of our analysis lies in the quantification of the range of the dispersion of the zero-flow pressure measurements and its contribution to the uncertainty in the estimated leakage airflow rate. Delmotte (2017) [16] as well as Prignon et al. (2019) [32] have recently stressed the importance of the zero-flow pressure in uncertainty analyses. Our results show that indeed, the contributions of the zero-flow pressure measurement and the measurement at the target pressure station have about the same size. Again, these results are limited to the few test cases we have examined; however, they reinforce previous authors' results as well as the need to better account for the zero-flow pressure error. Note that, to our knowledge, present pressurisation test protocols ignore this aspect.

Without appropriate measurement wind pressure data or models, restricting the analyses to a periodic wind with a simple relationship giving the wind pressures was convenient. Note that, assuming there is no time lag between the upstream and downstream wind signals, our conclusions regarding the sensitivity of the uncertainty to wind period can be extended to each mode of any wind velocity or wind pressures decomposed in Fourier series. Nevertheless, it is unclear how to tackle the time lag issue and how significant its impact could be.

We have proposed a non-dimensional formulation of the problem. Besides the fact that it reduces the number of parameters used in the kernel of the code and improves its stability, it is useful to understand the cross-influence of parameters, as shown in the analysis of inertial effects. This approach would also be useful for statistical analyses to identify key influencing parameters or to determine protocols that would minimise uncertainty, possibly using local climatic data. Finally, the dimensional analysis proves to be useful for our current work to design a laboratory experiment to investigate the validity of our model.

8 CONCLUSION

Our model allows one to simulate the dynamic behaviour of the airflow rates and state variables in an enclosure with sharp-edged openings subjected to a pressurisation test with periodic wind. This makes it possible to estimate the uncertainty on the air leakage coefficient. The analyses are restricted to one-point pressurisation tests at a given pressure station (DC pressurisation) in this paper but they could be extended to multi-point DC tests or alternative test methods such as AC or Pulse pressurisation. This would be useful because these other methods may give smaller uncertainties, in particular at low wind speed and low reference pressure. The fundamental equations would remain the same but some new analyses would be required to derive the airtightness characteristics from the airflow rate, pressure and temperature time series. Extending our model to other alternate flow models to better describe the flow behaviour in leaks (e.g., quadratic or power law) would require additional research efforts on the flow equations.

Our analyses show that a steady approach to uncertainties in building pressurisation tests is quite limited because the wind fluctuations can yield much larger uncertainties than the average wind alone. In addition, we have shown the significant impact of the wind frequency on the results and have confirmed that ignoring the zero-flow pressure uncertainty is inappropriate because of its significant contribution to the uncertainty of the leakage airflow rate error. Although our model has clear limitations, we expect these key conclusions generally hold in field pressurisation tests.

Overall, our approach could be used to develop pressurisation test protocols to minimise uncertainties, in parallel to investigating several aspects highlighted in this paper, including

555 the sensitivity of the results to the leakage flow model or the lack of adequate experimental
556 wind and pressurisation test data.
557

558 9 ACKNOWLEDGEMENTS

559 This research was initiated and funded in part by ICEE. The sole responsibility for the content
560 of this publication lies with the authors.
561

562 10 APPENDIX

563 10.1 Dimensionless groups

564 Let the non-dimensional numbers defined in Table 2.
565

$$t^* = t\,\frac{U_{ref}}{L_{ref}};\; f_w^* = \frac{L_{ref}}{U_{ref}} f_w$$

$$p_{abs,e}^* = \frac{p_{abs,e}}{p_{abs,0}}; p_{abs,i}^* = \frac{p_{abs,i}}{p_{abs,0}}; p_{abs,w}^* = \frac{\frac{\rho_0 U_{ref}^2}{2}}{p_{abs,0}}$$

$$\rho_e^* = \frac{\rho_e}{\rho_0}; \rho_i^* = \frac{\rho_i}{\rho_0}; \rho_{bd}^* = \frac{\rho_{pd}}{\rho_0};\; \rho_1^* = \frac{\rho_1}{\rho_0}; \rho_2^* = \frac{\rho_2}{\rho_0};$$

$$T_e^* = \frac{T_e}{T_0}; T_i^* = \frac{T_i}{T_0};\; T_{pd}^* = \frac{T_{pd}}{T_0};\; T_1^* = \frac{T_1}{T_0}; T_2^* = \frac{T_2}{T_0};$$

$$Fr_1 = \frac{U_{ref}}{\sqrt{g\, z_1}};\;\; Fr_2 = \frac{U_{ref}}{\sqrt{g\, z_2}}$$

$$Ld = \frac{C_{z,2}\, A_2}{C_{z,1}\, A_1}; F_1 = \frac{L_{ref}}{l_{e,1}}; F_2 = \frac{L_{ref}}{l_{e,2}}$$

$$G_{pd} = \frac{L_{ref}\left(C_{z,1}\, A_1 + C_{z,2}\, A_2\right)}{V_i}; G_1 = \frac{L_{ref}\, C_{z,1}\, A_1}{V_i}$$

$$q_{pd}^* = \frac{q_{pd}}{\left(C_{z,1}\, A_1 + C_{z,2}\, A_2\right) U_{ref}}; q_1^* = \frac{q_1}{C_{z,1}\, A_1\, U_{ref}};\; q_2^* = \frac{q_2}{C_{z,2}\, A_2\, U_{ref}}$$

$$q_{m,pd}^* = \rho_{pd}^*\, q_{pd}^*;\; q_{m,1}^* = \rho_1^*\, q_1^*; q_{m,2}^* = \rho_2^*\, q_2^*;$$
$$\Phi_{pd}^* = q_{m,pd}^*\, T_{pd}^*;\; \Phi_1^* = q_{m,1}^*\, T_1^*; \Phi_2^* = q_{m,2}^*\, T_2^*$$
$$U^* = \frac{U}{U_{ref}};\; c^* = \frac{c}{U_{ref}}$$

$$p_i^* = \frac{p_i}{\frac{\rho_0 U_{ref}^2}{2}}; p_s^* = \frac{p_s}{\frac{\rho_0 U_{ref}^2}{2}}; p_{w,ref}^* = \frac{p_{w,ref}}{\frac{\rho_0 U_{ref}^2}{2}}$$

$$C_{p,1} = \frac{C_{pw,1}\frac{\rho_e U^2}{2} - p_{w,ref}}{\frac{\rho_0 U_{ref}^2}{2}}; C_{p,2} = \frac{C_{pw,2}\frac{\rho_e U^2}{2} - p_{w,ref}}{\frac{\rho_0 U_{ref}^2}{2}}; \; C_{p,i} = \frac{p_i - p_{w,ref}}{\frac{\rho_0 U_{ref}^2}{2}}$$

$$\Delta p_1^* = \frac{\Delta p_1}{\frac{\rho_0 U_{ref}^2}{2}}; \Delta p_2^* = \frac{\Delta p_2}{\frac{\rho_0 U_{ref}^2}{2}}$$

Table 2: Non-dimensional numbers

10.2 Non-dimensional continuity and energy equations

The continuity and energy equations become:

$$\frac{d\rho_i^*}{dt^*} = \; G_{pd}\, \rho_{pd}^*\, q_{pd}^* + \; G_1\, \rho_1^*\, q_1^* + G_1\, Ld\, \rho_2^*\, q_2^* \tag{57}$$

$$\frac{1}{2}\frac{1}{c^{*2}}\frac{d\left(C_{p,i}\right)}{dt^*} = \; G_{pd}\, \rho_{pd}^*\, T_{pd}^*\, q_{pd}^* + \; G_1\, \rho_1^*\, T_1^*\, q_1^* + \; G_1\, Ld\, \rho_2^*\, T_2^*\, q_2^* \tag{58}$$

11 REFERENCES

[1] G.T. Tamura, Measurement of air leakage characteristics of house enclosures, ASHRAE Trans. (1975) 202–211.

[2] J. Jokisalo, J. Kurnitski, M. Korpi, T. Kalamees, J. Vinha, Building leakage, infiltration, and energy performance analyses for Finnish detached houses, Build. Environ. 44 (2009) 377–387. doi:10.1016/j.buildenv.2008.03.014.

[3] J.M. Logue, M.H. Sherman, I.S. Walker, B.C. Singer, Energy impacts of envelope tightening and mechanical ventilation for the U.S. residential sector, Energy Build. 65 (2013) 281–291. doi:10.1016/j.enbuild.2013.06.008.

[4] V. Leprince, A. Bailly, F.R. Carrié, M. Olivier, State of the Art of Non-Residential Buildings Air-tightness and Impact on the Energy Consumption, in: Proc. 32nd AIVC Conf. 12-13 Oct. 2011, Brussels, Belgium, 2011: pp. 12–13. http://www.aivc.org/sites/default/files/7b2.pdf.

[5] F. Richieri, B. Moujalled, T. Salem, F.R. Carrié, Airtightness impact on energy needs and airflow pattern: a numerical evaluation for mechanically ventilated dwellings in France, Int. J. Vent. 15 (2016) 134–150. doi:10.1080/14733315.2016.1203608.

[6] B. Jones, P. Das, Z. Chalabi, M. Davies, I. Hamilton, R. Lowe, A. Mavrogianni, D. Robinson, J. Taylor, Assessing uncertainty in housing stock infiltration rates and associated heat loss: English and UK case studies - ScienceDirect, Build. Environ. 92 (2015) 644–656. doi:https://doi.org/10.1016/j.buildenv.2015.05.033.

[7] M.H. Sherman, W.R. Chan, Building Airtightness: Research and Practice. Building Ventilation: The State of the Art Review, LBNL Rep. (2004).

[8] V. Leprince, F.R. Carrié, M. Kapsalaki, Building and ductwork airtightness requirements in Europe – Comparison of 10 European countries, in: Proc. 38th AIVC Conf. 13-14 Sept. 2017, Nottingham, UK, 2017.

[9] V. Leprince, M. Kapsalaki, F.R. Carrié, VIP N°37: Impact of Energy Policies on Building and Ductwork Airtightness, AIVC Vent. Inf. Pap. (2017). https://www.researchgate.net/publication/334391533_Ventilation_Information_Paper_n_37_Impact_of_Energy_Policies_on_Building_and_Ductwork_Airtightness.
[10] F.R. Carrié, S. Charrier, Building regulations can foster quality management — the French example on building airtightness, QUALICHeCK. (2015). http://qualicheck-platform.eu/2015/02/fact-sheet-01-building-regulations-can-foster-quality-management/.
[11] ISO, EN ISO 9972: Thermal performance of buildings - Determination of air permeability of buildings - Fan pressurization method, (2015).
[12] F.R. Carrié, P. Wouters, Building airtightness: a critical review of testing, reporting and quality schemes in 10 countries, AIVC Tech. Note. 67 (2012).
[13] ASTM, E779-19 Standard Test Method for Determining Air Leakage Rate by Fan Pressurization, ASTM Int. (2019). doi:10.1520/E0779-19.
[14] I.S. Walker, M.H. Sherman, J. Joh, W.R. Chan, Applying Large Datasets to Developing a Better Understanding of Air Leakage Measurement in Homes, Int. J. Vent. 11 (2013). https://www.tandfonline.com/doi/abs/10.1080/14733315.2013.11683991.
[15] F.R. Carrié, V. Leprince, Uncertainties in building pressurisation tests due to steady wind, Energy Build. 116 (2016) 656–665. doi:10.1016/j.enbuild.2016.01.029.
[16] C. Delmotte, Airtightness of Buildings–Considerations regarding the Zero-Flow Pressure and the Weighted Line of Organic Correlation, in: Proc. 38th AIVC Conf. 13-14 Sept. 2017, Nottingham, UK, 2017.
[17] C. Delmotte, J. Laverge, Interlaboratory tests for the determination of repeatability and reproducibility of buildings airtightness measurements, in: Proc. 32nd AIVC Conf. 12-13 Oct. 2011, Brussels, Belgium, 2011.
[18] C. Delmotte, Airtightness of buildings-Calculation of combined standard uncertainty, in: Proc. 34th AIVC Conf. 24-25 Sept. 2014, 2013.
[19] A.K. Persily, Repeatability and accuracy of pressurization testing, in: Proc. ASHRAE-DOE Conf. Dec 6-9 1982, USA, 1982: pp. 380–390.
[20] A.K. Persily, Air flow calibration of buildings pressurization devices, NBS Rep. NBSIR 84-2849 (1984).
[21] A.K. Persily, R.A. Grot, Accuracy in Pressurization Data Analysis, ASHRAE Trans. (1984).
[22] D.W. Etheridge, Air leakage characteristics of houses—a new approach, Build. Serv. Eng. Res. Technol. 5 (1984) 32–36.
[23] K.J. Gadsby, D.T. Harrje, Fan pressurization of buildings: Standards, calibration, and field experience, ASHRAE Trans U. S. 91:2B (1985). https://www.osti.gov/biblio/5552192.
[24] P. duPont, Blower doors: variation in leakage measurements, Energy Audit. Retrofit. (1986) 7–10.
[25] M.P. Modera, D.J. Wilson, The Effects of Wind on Residential Building Leakage Measurements, Air Change Rate Airtightness Build. -. ASTMSTP 1067 (1990). doi:10.1520/STP17210S.
[26] M. Sherman, L. Palmiter, Uncertainties in Fan Pressurization Measurements, Airflow Perform. Build. Envel. Compon. Syst. (1994). doi:10.1520/STP14701S.
[27] K. Siren, A modification of the power-law equation to account for large scale wind turbulence, in: Proc. 18th AIVC Conf. 23-24 Sept. 1997, Athens, Greece, 1997. https://www.aivc.org/resource/modification-power-law-equation-account-large-scale-wind-turbulence.
[28] M. Sherman, A Power-Law Formulation of Laminar Flow in Short Pipes, J. Fluids Eng. 114 (1992) 601–605. doi:10.1115/1.2910073.

[29] I.S. Walker, D.J. Wilson, M.H. Sherman, A comparison of the power law to quadratic formulations for air infiltration calculations, Energy Build. 27 (1998) 293–299. doi:10.1016/S0378-7788(97)00047-9.
[30] E. Cooper, X. Zheng, C. Wood, M. Gillot, D. Tetlow, S. Riffat, L. De Simon, Field trialling of a pulse airtightness tester in a range of UK homes, J. Vent. 18 (2016). https://www.tandfonline.com/doi/full/10.1080/14733315.2016.1252155 (accessed June 18, 2019).
[31] F.R. Carrié, V. Leprince, Model error due to steady wind in building pressurization tests, in: Proc. 35th AIVC Conf. 24-25 Sept. 2014, Poznan, Poland, 2014.
[32] M. Prignon, A. Dawans, S. Altomonte, G. Van Moeseke, A method to quantify uncertainties in airtightness measurements: Zero-flow and envelope pressure, Energy Build. 188–189 (2019) 12–24. doi:10.1016/j.enbuild.2019.02.006.
[33] D.W. Etheridge, Unsteady flow effects due to fluctuating wind pressures in natural ventilation design—mean flow rates, Build. Environ. 35 (2000) 111–133.
[34] D.W. Etheridge, Unsteady flow effects due to fluctuating wind pressures in natural ventilation design—instantaneous flow rates, Build. Environ. 35 (2000) 321-337111–133.
[35] D.W. Etheridge, M. Sandberg, Building Ventilation: Theory and Measurement, JOHN WILEY & SONS, JOHN WILEY & SONS, 1996. https://www.wiley.com/en-us/Building+Ventilation%3A+Theory+and+Measurement-p-9780471960874 (accessed November 12, 2018).
[36] M.P. Modera, Periodic flow through thin-plate slots., Doctoral Dissertation, Dept. of heating and Ventilating, Royal institue of Tehcnology of Stockholm, 1989.
[37] F.R. Carrié, Temperature and pressure corrections for power-law coefficients of airflow through ventilation system components and leaks, in: Proc. 35th AIVC Conf. 24-25 Sept. 2014, Poznań, Poland, 2014.
[38] M.W. Liddament, A Guide to Energy Efficient Ventilation - AIC-TN-VENTGUIDE-1996, (1996) 254 pp.
[39] BIPM, JCGM 100:2008 - Evaluation of measurement data - Guide to the expression of uncertainty in measurement, (2008).
[40] T. Brennan, G. Nelson, C. Olson, Repeatability of Whole-Building Airtightness Measurements: Midrise Residential Case Study, in: Proc. AIVC Int. Workshop April 18-19 2013, Washington D.C, 2013.
[41] M.P. Modera, M.H. Sherman, AC pressurization: a technique for measuring leakage area in residential buildings, in: Proc. Am. Soc. Heat. Refrig. Air-Cond. Eng. Semiannu. Meet. 23 Jun 1985, Honolulu, HI, USA, 1985.
[42] M. Sherman, M. Modera, Low-frequency measurement of leakage in enclosures, Rev. Sci. Instrum. 57 (1986) 1427–1430. doi:10.1063/1.1138615.
[43] M.H. Sherman, M.P. Modera, Signal Attenuation Due to Cavity Leakage | Energy Technologies Area, J. Acoust. Soc. Am. 84 (1988). https://eta.lbl.gov/publications/signal-attenuation-due-cavity-leakage (accessed June 18, 2019).